HYDROLOGICAL PROCESSES
Hydrol. Process. **22**, 2063–2074 (2008)
Published online 4 October 2007 in Wiley InterScience
(www.interscience.wiley.com) DOI: 10.1002/hyp.6806

Linking runoff response to burn severity after a wildfire†

John A. Moody,[1]* Deborah A. Martin,[1] Sandra L. Haire[2] and David A. Kinner[3]

[1] *US Geological Survey, Water Resources Discipline, 3215 Marine St., Suite E-127, Boulder, CO 80303, USA*
[2] *Holdsworth Natural Resources Center, University of Massachusetts, Amherst, MA 01003, USA*
[3] *Western Carolina University, Cullowhee, NC 28723, USA*

Abstract:

Extreme floods often follow wildfire in mountainous watersheds. However, a quantitative relation between the runoff response and burn severity at the watershed scale has not been established. Runoff response was measured as the runoff coefficient C, which is equal to the peak discharge per unit drainage area divided by the average maximum 30 min rainfall intensity during each rain storm. The magnitude of the burn severity was expressed as the change in the normalized burn ratio. A new burn severity variable, hydraulic functional connectivity Φ was developed and incorporates both the magnitude of the burn severity and the spatial sequence of the burn severity along hillslope flow paths. The runoff response and the burn severity were measured in seven subwatersheds (0·24 to 0·85 km^2) in the upper part of Rendija Canyon burned by the 2000 Cerro Grande Fire near Los Alamos, New Mexico, USA.

A rainfall–discharge relation was determined for four of the subwatersheds with nearly the same burn severity. The peak discharge per unit drainage area Q_u^{peak} was a linear function of the maximum 30 min rainfall intensity I_{30}. This function predicted a rainfall intensity threshold of 8·5 mm h^{-1} below which no runoff was generated. The runoff coefficient $C = Q_u^{peak}/I_{30}$ was a linear function of the mean hydraulic functional connectivity of the subwatersheds. Moreover, the variability of the mean hydraulic functional connectivity was related to the variability of the mean runoff coefficient, and this relation provides physical insight into why the runoff response from the same subwatershed can vary for different rainstorms with the same rainfall intensity. Published in 2007 by John Wiley & Sons, Ltd.

KEY WORDS runoff response; burn severity; wildfire; connectivity; peak discharge

Received 6 November 2006; Accepted 1 May 2007

INTRODUCTION

The runoff response from burned watersheds is a function of rainfall and soil properties. Rainfall in mountainous terrain is often characterized by complex temporal and spatial patterns (Rowe *et al*., 1954; Robichaud and Waldrop, 1994; Moody and Martin, 2001a) superimposed on the land surface. Fires change the spatially heterogeneous patterns of soil properties, vegetation layers, and topography at the land surface. This heterogeneity can be visualized as a mosaic of soil patches each with homogenous characteristics, such as antecedent moisture, sorptivity, and saturated hydraulic conductivity (Smith *et al*., 2002). Some patches generate overland flow by rainfall excess and other patches are sinks (Kutiel *et al*., 1995) where overland flow infiltrates. These patches (Morin and Kosovsky, 1993) are connected by hydrologic properties (Nachabe *et al*., 1997; Davenport *et al*., 1998; Darboux *et al*., 2001) and by overland flow to produce a sequence of hillslope flow paths that control the runoff from a burned watershed.

Prediction of the runoff response from burned watersheds is hampered at the present time by the lack of adequate data. Most rainfall–runoff prediction methods have been developed for unburned watersheds (Hawkins, 1973; Interagency Advisory Committee on Water Data, 1981; NRCS, 1986; Feldman, 2000; Ries and Crouse, 2002); however, without adequate data to verify these methods for burned watersheds their reliability as predictive tools is uncertain. Despite these limitations, land-management agencies have been required to assess the risks of floods from burned watersheds, and this has led to published predictions of runoff and erosion from burned watersheds without field verification (BAER, 2000, 2002; Miller *et al*., 2003).

Burn severity is an important variable that has been identified in the fire literature as affecting the runoff response. Thus, in the hydrologic sense (used in this paper), the burn severity should represent the fire effects on vegetation and soil characteristics that subsequently determine the runoff response. Usually, burn severity has been classified into discrete descriptive classes such as high, moderate, and low burn severity (National Wildfire Coordinating Group, 1994). These classes are assumed to reflect the degree of removal of the canopy layer, which intercepts rainfall (Zinke, 1967), as well as the removal of the understorey, ground cover, litter, and duff layers, all of which create obstructions and increase frictional drag (Gilley *et al*., 1992) during surface runoff. Also, the burn severity alters the infiltration properties of the soil (DeBano, 2000; Smith *et al*., 2002; Moody *et al*.,

* Correspondence to: John A. Moody, US Geological Survey, Water Resources Discipline, 3215 Marine St., Suite E-127, Boulder, CO 80303, USA. E-mail: jamoody@usgs.gov

2005) and, thus, indirectly affects the runoff response. These descriptive classes of burn severity, however, are not suitable for use in mathematical equations to predict the magnitude of the runoff response.

Recently, continuous quantitative measures or metrics of the magnitude of the burn severity have been developed using remotely sensed data. One such metric is the change in the normalized burn ratio ΔNBR (Key and Benson, 2005), which incorporates reflectance measurements from Landsat imagery and was designed to measure the fire effects on vegetation and soil characteristics. In this paper, we use this burn severity metric: (1) to determine a relation between rainfall and runoff response in burned watersheds; (2) to test the hypothesis that the runoff response is a function of both the magnitude of the burn severity and the spatial sequence of this burn severity along a hillslope flow path.

BACKGROUND

Burn severity and runoff response were measured in the Rendija Canyon watershed burned by the 2000 Cerro Grande Fire. The fire burned 173 km^2 across the eastern side of the Jemez Mountains near and in Los Alamos, New Mexico, USA. This included 12·5 km^2 in the Rendija Canyon where, in the upper part, about 82% of the watershed burned at high severity, 10% at moderate severity, 6% at low severity, and 2% was unburned (BAER, 2000). Upper Rendija Canyon drains eastward across the Pajarito Plateau towards the Rio Grande. The maximum elevation is 3000 m and the outlet is at 2190 m. The Jemez Mountains have a summertime convective rainfall regime (Bowen, 1990) with a summer July–September rainfall gradient (Reneau *et al*., 2003) ranging from 280 mm near the mountain crest (3000 m) to 150 mm near the edge of the plateau (1750 m). Estimates of the 2-year, 5-year, 10-year, and 100-year recurrence intervals for the 30 min rainfall intensities are 34 mm h^{-1}, 46 mm h^{-1}, 55 mm h^{-1}, and 85 mm h^{-1} respectively (Miller *et al*., 1973; Reneau *et al*., 2003; Bonnin *et al*., 2004). The study area (7·53 km^2) in the upper part of Rendija Canyon (Figure 1) was subdivided into 15 subwatersheds ranging in size from 0·24 to 0·85 km^2 (Table I).

METHODS

Watershed characteristics

Topographic and hydraulic variables were determined from a 30 m digital elevation model (DEM). We used part of the 7·5′ Guaje Mountain quadrangle in New Mexico (1 : 24 000). Elevation, slope, flow accumulation, and flow direction were calculated for each 30 m pixel using computer software (ArcInfo Environmental Systems Research Institute, version 8·3). Slopes along hillslope flow paths were computed using the length or diagonal of each pixel, depending on the flow direction. The location and areal extent of bedrock outcrops were measured on 1 : 6000 aerial photographs of Rendija Canyon taken either on 21 July 2000 (black and white) or on 26 August 2002 (colour).

Runoff response

The runoff coefficient, which depends on the peak discharge, the drainage area, and the rainfall intensity, was used to measure the runoff response. It explicitly includes and normalizes for the fact that different rainfall intensities may be superimposed on different subwatersheds during the same rainstorm. Stream gauges were

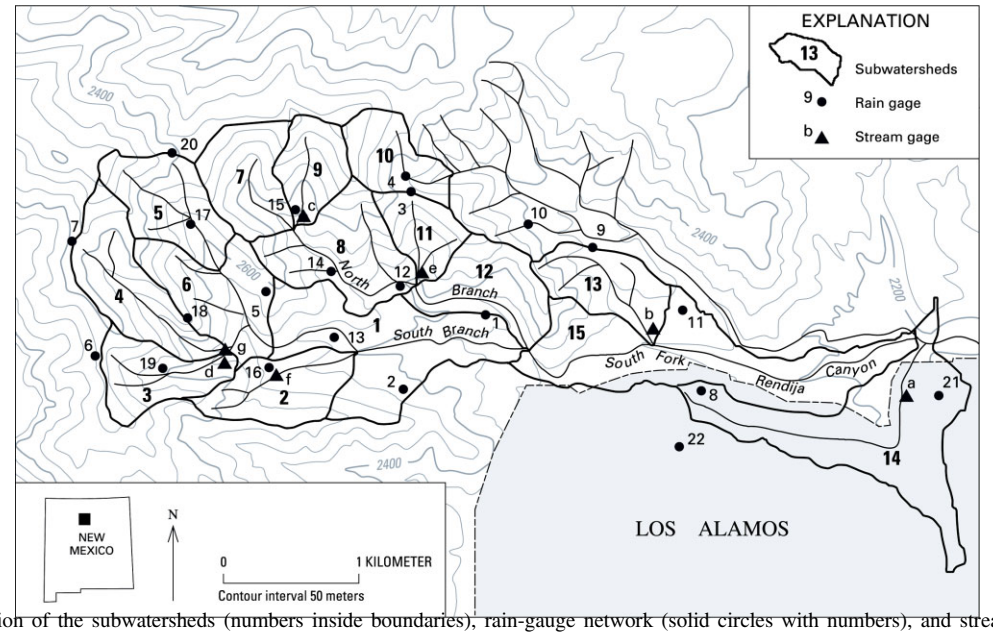

Figure 1. Location of the subwatersheds (numbers inside boundaries), rain-gauge network (solid circles with numbers), and stream-gauge network (solid triangles with lower case letters) in Rendija Canyon. The rain-gauge network had 20 gauges in 2001 (numbers 1–20) and 22 gauges in 2002 (numbers 1–23 minus number 4). The stream-gauge network had four gauges in 2001 (letters a–d) and seven gauges in 2002 (letters a–g)

Published in 2007 by John Wiley & Sons, Ltd.

DOI: 10.1002/hyp

Table I. Characteristics of selected subwatersheds in Rendija Canyon[a]

Sub-watershed	Elevation (m)			Drainage area		Burn severity[a]		I_{30}^{thresh} (mm h^{-1})	
	Outlet	Maximum	Range	Upstream from measurement site (km^2)	Covered by bedrock outcrops (%)	ΔNBR	CV	2001	2002
2	2440	2676	236	0·26	2·7	730	0·15	—	12
3	2540	2792	252	0·31	0·4	589	0·29	5·3	8·7
4	2520	2999	479	0·50	1·1	383	0·50	2·2	14
9	2520	2816	296	0·25	2·2	547	0·30	4·6	18
11	2400	2697	297	0·24	2·0	615	0·10	—	18
13	2260	2524	263	0·33	4·8	574	0·21	7·3	10·4
14[b]	2190	2207	17	0·85	9·9	30	3·47	4·0	7·1

[a] ΔNBR is before–after change in the normalized burn ratio; CV is coefficient of variation of ΔNBR.
[b] Bedrock outcrops represent paved surfaces.

deployed in subwatersheds with a range of burn severities to measure the peak water depth h^{peak} corresponding to the peak discharge, and a network of rain-gauges was deployed to measure rainfall intensity (Figure 1). The runoff coefficient C is defined by the rational equation, which provides a simple equation to begin to investigate the link between runoff response and burn severity. It is the dimensionless proportionality constant in the relation between discharge Q (m^3 s^{-1}), rainfall intensity I (mm h^{-1}), and contributing area A_c (m^2) and is given by Chow (1964) as

$$Q = CIA_c \tag{1}$$

This runoff coefficient incorporates the effects of many variables, such as antecedent moisture, sorptivity, saturated hydraulic conductivity, topographic slope, roughness, and channel network properties. Burn severity is the primary variable investigated in this paper and is linked to some of these variables. In a field experiment of this nature it is impossible to control all possible variables, but some variables were controlled by choosing subwatersheds that were relatively close. One can then assume, for example, that the antecedent moisture conditions might be the same before each storm and that the water infiltration characteristic curves for the soil may be similar given the similar bedrock geology and elevation.

The rational equation is applicable for small, burned watersheds (G. Kuyumjian, personal communication, 2005) similar to those in the study area and assumes that the duration of uniform rainfall intensity is long enough so that the contributing area is equal to the total drainage area (Barfield and Warner, 1985). This was assumed to be true at peak discharge; so, by substituting the peak discharge for Q in Equation (1) and dividing both sides by the total drainage area, gives the peak discharge per unit drainage area Q_u^{peak} as

$$Q_u^{peak} = CI \tag{2}$$

Values of Q_u^{peak} have been shown to be a function of the rainfall intensity (Moody and Martin, 2001b), so that the runoff response between different watersheds can only be compared for the same rainfall intensity. Substitution of I_{30} for I in Equation (2) and solving for the dimensionless runoff coefficient gives

$$C = \frac{Q_u^{peak}}{I_{30}} \tag{3}$$

Peak discharge. Peak discharges from the subwatersheds were computed by assuming critical flow at the measurement cross-section. The cross-sectional mean peak velocity v^{peak} (m s^{-1}) in a channel based on the critical flow assumption is

$$v^{peak} = (gh^{peak})^{1/2} \tag{4}$$

where $g = 9{\cdot}8$ m s^{-2} is the acceleration due to gravity. Critical flow has been shown by Jarrett (1987) and Grant (1997) to model flow conditions characterized by high-gradient streams with abundant sediment in mobile beds of sand and gravel. They also have argued for critical flow in mountainous streams characterized by high relative roughness where particle diameters of bed material are on the order of the flow depth. These large particles extract energy from the mean flow in the form of turbulence creating a hydraulic 'brake' on flow accelerations especially in step–pool systems. Channels in burned watersheds after the first flood, and definitely those in Rendija Canyon, frequently have mobile beds, large relative roughness, and debris and boulders that create step–pool systems. This was also true after the 1996 Buffalo Creek Fire in Colorado, and critical flow was used to model measured discharges in the mountainous channels of Buffalo and Spring Creeks (Moody and Martin, 2001a) where the channel slopes were steep (~0·04) and similar to the channel slopes in Rendija Canyon. The peak discharge Q^{peak} is then given by

$$Q^{peak} = v^{peak}a \tag{5}$$

where a (m^2) is the cross-sectional area of the channel at peak discharge.

The cross-sectional area was calculated from bed-surface measurements and the peak water-depth. We used a standard self-compensating level to measure bed-surface elevations with a vertical accuracy of 0·01 m

and a horizontal accuracy of 0·1 m. Aware of the ephemeral nature of floods after wildfires, we wanted to maximize the number of measurements of peak discharge; therefore, we could not establish all discharge measuring sections at sites with a stable cross-section, which is a common practice in unburned watersheds. We used the cross-sectional area measured before a flood as the best estimator. We assumed little erosion (change in channel cross-sectional area) during the rising limb of the hydrograph, when form drag from large bank and bed roughness decreases the excess shear stress. At peak discharge, the water depth and, consequently, the excess shear stress are a maximum and erosion and sediment transport are probably a maximum. After peak discharge, the cross-sectional area continues to change rapidly as the eroded sediment is deposited.

The peak water-depth h^{peak} was determined by using high-water marks (HWs) and recording pressure sensors, which recorded pressure every 2 min. HWs were affected by surface waves (Figure 2) created by the high relative roughness in the channels and represented the elevation of the highest wave while the pressure sensors filtered out these waves.

Uncertainty estimates for each $Q_{\text{u}}^{\text{peak}}$ measurement were calculated as the sum of square variances of the peak water-depth, cross-sectional area, and the drainage area. A linear adjustment was determined for the peak discharges based on HWs by correlating 30 paired measurements of peak water discharge based on HWs and based on pressure sensors made at identical times. The linear adjustment equation was

$$Q_{\text{u}}^{\text{peak}}(\text{pressure}) = 0{\cdot}28 Q_{\text{u}}^{\text{peak}}(\text{HW}) \quad R^2 = 0{\cdot}56 \qquad (6)$$

Therefore, in the case of measurements based on the HWs, the uncertainty (variance) introduced by using the adjustment equation was included in the final uncertainty of $Q_{\text{u}}^{\text{peak}}$.

Figure 2. Photograph of the turbulent flow in Rendija Canyon. The diameters of the trees in the channel are 0·2–0·3 m. View is downstream. Photograph was taken by Thomas Trujillo

Rainfall intensity. Little is known about the size or spatial variability of convective storms in mountainous regions. Considering previous results (Huff, 1979; Goodrich *et al.*, 1995; May and Julien, 1998) in different regions, one recording tipping-bucket rain-gauge was deployed in each subwatershed or within 100 m of the boundary of a subwatershed. The density of rain-gauges was 2·6 km^{-2} and 2·9 km^{-2} in 2001 and 2002 respectively (Figure 1). These rain-gauges had a 0·152 m diameter opening (Onset, model RG-1 and RG-2), were calibrated in the laboratory, and were used to measure both the total rainfall and rainfall intensity. The gauges recorded the time of each tip with a volume equivalent to 0·254 mm of rain.

The maximum 30 min rainfall intensity was used to characterize convective rainstorms. About 80% of the total rainfall for a convective storm falls in the first 30 min (Hershfield, 1961; Miller *et al.*, 1973). Rainfall intensities were not uniform over the subwatersheds; therefore, the area-weighted average of the maximum 30 min rainfall intensity I_{30} associated with runoff from each subwatershed was computed using the isohyetal method (Barfield and Warner, 1985). Uncertainties in the natural variability of the rainfall intensity (Table II) were equal to the standard deviation of the values of rainfall intensity measured at the primary rain-gauge in a subwatershed and the rainfall intensity measured at four to seven of the nearest rain-gauges surrounding the primary gauge. A rainfall-intensity threshold I_{30}^{thres} was estimated for some subwatersheds. The pressure sensors acted as a detector of surface and subsurface flow in the channels. Positive pressure indicated surface flow, whereas negative pressures (caused by capillary tension in the alluvial sand filling the channels) indicated subsurface flow. The threshold rainfall intensity was defined as the largest value of I_{30} (Table I) below which no surface flow was detected by the pressure sensors.

Burn severity

Burn severity was quantified as the change in the normalized burn ratio ΔNBR. This ratio is derived from remote-sensing measurements of Earth radiation (Landsat Thematic Mapper and Landsat ETM+ data). Raw digital values for spectral band 4 (R_4) and band 7 (R_7) are converted to radiance and then to at-satellite reflectance before computing the normalized burn ratio NBR (Key and Benson, 2005):

$$\text{NBR} = 1000\frac{R_4 - R_7}{R_4 + R_7} \qquad (7)$$

NBR represents a normalized difference of two spectral bands sensitive to fire effects. Band 4 in the near infrared, $(0{\cdot}76–0{\cdot}90) \times 10^{-6}$ m, measures the reflected radiation from vegetation, which typically decreases as a consequence of fire. Band 7 in the short-wave infrared, $(2.08–2.35) \times 10^{-6}$ m, measures the reflected radiation from bare soil, which typically increases as a consequence of fire (Benavides-Solorio and MacDonald, 2005). To calculate the change in the normalized burn

Table II. Discharge per unit drainage area and rainfall intensity for 2001 and 2002 in seven subwatersheds of Rendija Canyon[a]

Watershed	Date	ΔNBR = 581 ± 5%					Watershed	Date	ΔNBR ≠ 581 ± 5%				
		Discharge per unit drainage area ($m^3\ s^{-1}\ km^{-2}$)			Rainfall intensity I_{30} ($mm\ h^{-1}$)				Discharge per unit drainage area ($m^3\ s^{-1}\ km^{-2}$)			Rainfall intensity I_{30} ($mm\ h^{-1}$)	
		Average	Uncertainty	*N*	Area weighted	Uncertainty			Average	Uncertainty	*N*	Area weighted	Uncertainty
Watersheds in 2001													
3	2 Jul	7·50	1·01	4	52·7	19·2	2	2 Jul	21·49	2·61	3	70·4	17·2
3	13 Jul	1·65	0·33	1	22·3	5·4	2	13 Jul	1·90	0·39	1	15·3	6·8
3	1 Aug	0·00076	0·000033	1	5·4	0·4	2	24 Jul	2·07	0·43	1	10·0	2·7
3	8 Aug	0·0196	0·001	2	10·5	2·2	2	26 Jul	19·06	2·28	3	54·0	13·2
3	9 Aug	4·43	0·74	2	38·0	2·3	2	9 Aug	3·33	0·49	2	36·7	5·6
3	11 Aug	0·44	0·019	1	10·8	22·4	2	11 Aug	1·15	0·24	1	44·5	19·6
3	14 Aug	0·39	0·017	1	12·6	3·0							
9	2 Jul	0·45	0·179	1	22·8	19·0	4	2 Jul	1·26	0·42	2	26·8	19·9
9	26 Jul	8·50	1·30	3	36·8	12·4	4	13 Jul	0·90	0·42	1	28·5	8·2
9	8 Aug	0·43	0·17	1	11·0	4·7	4	26 Jul	3·30	1·09	2	30·4	9·3
9	9 Aug	0·31	0·12	1	15·0	4·6	4	8 Aug	2·70	1·26	1	13·3	5·0
9	11 Aug	1·68	0·26	3	22·9	14·0	4	9 Aug	5·20	1·719	2	36·4	7·5
9	14 Aug	0·20	0·080	1	5·0	3·9							
9	16 Aug	1·93	0·44	3	7·6	2·1							
11	23 Jun	0·023	0·0037	2	4·5	3·6	14	2 Jul (a)	0·21	0·052	2	22·9	6·0
11	2 Jul	5·04	1·45	3	43·0	13·0	14	2 Jul (b)	0·17	0·10	1	29·5	11·8
11	13 Jul	0·19	0·06	1	8·8	1·5	14	4 Aug	0·12	0·072	1	8·6	2·6
11	24 Jul	0·15	0·05	1	7·6	4·5	14	16 Aug	0·15	0·064	2	5·6	1·3
11	26 Jul	3·64	1·18	1	32·9	17·0							
11	11 Aug	3·64	1·18	1	32·5	5·2							
11	14 Aug	0·95	0·31	1	9·2	3·2							
13	2 Jul (a)	0·71	0·026	1	16·5	6·0							
13	2 Jul (b)	1·99	0·052	2	28·7	11·8							
13	2 Jul (c)	0·47	0·017	1	28·0	15·8							
13	11 Jul	0·43	0·016	1	18·5	9·4							
13	12 Jul	0·24	0·009	1	9·2	4·2							

Published in 2007 by John Wiley & Sons, Ltd.
Hydrol. Process. **22**, 2063–2074 (2008)
DOI: 10.1002/hyp

Table II. (*Continued*)

Watershed	Date	ΔNBR = 581 ± 5%					Watershed	Date	ΔNBR ≠ 581 ± 5%				
		Discharge per unit drainage area ($m^3\ s^{-1}\ km^{-2}$)			Rainfall intensity I_{30} ($mm\ h^{-1}$)				Discharge per unit drainage area ($m^3\ s^{-1}\ km^{-2}$)			Rainfall intensity I_{30} ($mm\ h^{-1}$)	
		Average	Uncertainty	*N*	Area weighted	Uncertainty			Average	Uncertainty	*N*	Area weighted	Uncertainty
13	26 Jul	0·20	0·007	1	11·6	5·1							
13	5 Aug	0·31	0·008	2	8·7	1·1							
13	11 Aug	2·89	0·075	2	32·5	12·5							
13	14 Aug	0·14	0·004	2	8·8	3·2							
13	16 Aug	1·27	0·027	3	7·0	2·2							
Watersheds in 2002													
3	21 Jun	3·78	0·59	3	49·9	11·5	2	21 Jun	3·77	0·45	3	58·0	9·8
3	22 Jun (a)	0·26	0·10	1	16·2	1·1	2	22 Jun (b)	0·26	0·05	1	12·4	2·2
3	22 Jun (b)	0·043	0·01	1	14·2	1·1	2	18 Jul	0·28	0·06	1	55·7	8·2
3	18 Jul	0·90	0·24	1	28·2	11·0	2	25 Jul	0·42	0·09	1	21·9	11·8
3	7 Aug	1·00	0·26	1	18·9	6·1	2	7 Aug	0·39	0·08	1	22·0	8·5
3	18 Aug	0·50	0·13	1	16·1	14·0	2	18 Aug	0·65	0·13	1	33·3	14·0
9	21 Jun	7·43	1·23	5	42·3	6·3	4	21 Jun	0·17	0·039	1	40·7	11·5
9	22 Jun (b)	3·10	1·59	1	17·4	4·5							
9	4 Jul	0·031	0·012	1	15·7	6·7	14	21 Jun	0·12	0·056	1	18·0	11·6
							14	22 Jun (a)	0·37	0·061	3	35·0	6·9
11	21 Jun	5·69	0·67	4	41·3	7·4	14	22 Jun (b)	0·00848	0·013	1	7·5	1·8
11	22 Jun (a)	1·60	0·20	1	18·4	1·0	14	22 Jul	0·060	0·036	1	7·2	3·8
11	22 Jun (b)	0·41	0·05	1	14·4	1·8	14	31 Jul	0·13	0·055	2	35·5	10·5
11	31 Jul	1·33	0·32	3	23·7	11·8							
13	21 Jun	0·93	0·049	1	26·9	11·3							
13	22 Jun (a)	1·08	0·40	3	26·1	7·7							
13	24 Jul	0·10	0·005	1	13·0	5·8							
13	31 Jul	1·58	0·048	3	45·0	6·8							

[a] All discharges are based on the critical flow assumption; uncertainty of rainfall intensity is the standard deviation of the data from the rain-gauge in the watershed and the surrounding rain-gauges for each rainstorm; uncertainty of the discharge is the standard deviations of measurements made using cross-sections measured before and after the flood; where no before–after pair was available, the average for the specific watershed was used; the uncertainty in discharge represents the worst case of change in the bed elevation.

Published in 2007 by John Wiley & Sons, Ltd.
Hydrol. Process. **22**, 2063–2074 (2008)
DOI: 10.1002/hyp

ratio ΔNBR, two images for June (one before the fire and one after) were selected so that the requirement of similar phenology was satisfied (Key and Benson, 2005) and so that the differences would provide the best measure of burn severity for hydrologic purposes. The post-fire image (4 June 2001) indicated some areas of 'green up' from seed germination and resprouting of shrubs corresponding to less burn severity that was not detected in an earlier image (September 2000), which indicated bare ground. The 4 June image provided a more accurate measurement of burn severity effect on hydrologic properties than the earlier post-fire image (September 2000). The NBR value within each pixel of the post-fire image (4 June 2001) was subtracted from the NBR value in the corresponding pixel of the pre-fire image (7 June 1999):

$$\Delta\mathrm{NBR} = \mathrm{NBR}_{\mathrm{prefire}} - \mathrm{NBR}_{\mathrm{postfire}} \tag{8}$$

Values of ΔNBR typically ranged from −1000 (indicating enhanced productivity) to +1000 (high burn severity) and for unburned areas often fall between −150 and +150. The values of ΔNBR have been correlated with the composite burn index (a field rating of burn severity) at other burns in the western USA (Cocke *et al*., 2005; Sorbel and Allen, 2005; Key and Benson, 2006). A mean value of ΔNBR was computed for each subwatershed (Table I).

Hydraulic functional connectivity. Values of ΔNBR do not include any information about the spatial connectivity of the burn severity within the subwatersheds. In order to develop a burn severity variable that includes the spatial connectivity, we have adapted the ecological concept of functional connectivity (McGarigal *et al*., 2002). This differs from the concept of structural connectivity in that it explicitly references a process (Peterson, 2002; McGarigal *et al*., 2002), which in this case is the runoff process. It has been shown that on unburned slopes the maximum runoff response develops when the infiltration capacity decreases down the hillslope (Hawkins and Cundy, 1987; Nachabe *et al*., 1997); and this is probably true for burned slopes, where infiltration capacity has been shown to be related to burn severity (DeBano, 2000; Martin and Moody, 2001; Doerr *et al*., 2006). In a digital flow model, all the runoff must traverse the last pixel before reaching the channel; hence, the last pixel should be weighted more than the first pixel near the watershed divide, where only a small fraction of the water traverses the pixel.

The hydraulic functional connectivity is based on simplifications of the hillslope runoff process. The hillslope discharge per unit width q ($\mathrm{m^2\ s^{-1}}$) is given by the product of the flow depth h (m) and the overland flow velocity w ($\mathrm{m\ s^{-1}}$), so that using a Darcy–Weisbach resistance equation (Bathurst, 1985; Abrahams *et al*., 1986; Moore and Foster, 1990) gives

$$q = wh = \left(\frac{8g}{f}\right)^{1/2} h^{3/2} s^{1/2} \tag{9}$$

where f is the Darcy–Weisbach friction factor and s is the slope associated with each pixel composing the hillslope flow path. On a burned hillslope, the expressions involving the friction factor f and the flow depth h are assumed to be functions of the burn severity; however, the exact relations are unknown. So, as a first-order approximation, the expression $(8g/f)^{1/2}h^{3/2}$ for each pixel i in the flow path was assumed to be proportional to $\Delta\mathrm{NBR}_i$.

The hydraulic functional connectivity is proportional to the discharge from each flow path into the main channel and was computed for a random sample of hillslope flow paths in each subwatershed. The start of each flow path was either in a pixel on the outer subwatershed divide or on an internal divide between channels. Following each hillslope flow path j composed of k connected pixels, the dimensionless hydraulic functional connectivity Φ_j was computed as follows:

$$\Phi_j = \frac{\sum_{i=1}^{k} \alpha_{ij} \Delta\mathrm{NBR}_{ij} s_{ij}^{1/2}}{\alpha} \tag{10}$$

where α_{ij} is a weighting factor equal to the uphill contributing area to pixel i in flow path j, s_{ij} is the local slope from pixel i to the next downstream pixel in flow path j, and α is the total area of the flow path. To illustrate the importance of the sequence of pixels encountered by water flowing along a hillslope flow path, we can assume a simple hypothetical flow path with a constant slope, pixel area equal to unity, a total area of four pixels. If the downhill sequence of $\Delta\mathrm{NBR}_i$ is 700, 500, 300, and 100, then $\Phi_j = 750$; but if the downhill sequence is reversed, with the most severely burned pixel closest to the channel, then the hydraulic functional connectivity $\Phi_j = 1250$.

The total discharge per unit area from a subwatershed can then be represented by the sum of the Φ_j values for each flow path normalized by the number of flow paths (Table III). Thus, the watershed hydraulic functional connectivity Φ is defined as the arithmetic average of Φ_j for N hillslope flow paths, or

$$\Phi = \frac{1}{N} \sum_{j=1}^{N} \Phi_j \tag{11}$$

At the 30 m pixel scale (determined by the Landsat imagery) it is impossible to resolve the detailed drainage network on hillslopes, but the pattern of burn severity is imprinted over the drainage network such that the burn severity variable, i.e. hydraulic functional connectivity, provides a first-order estimate of the spatial changes in burn severity along a hillslope flow path.

RESULTS AND DISCUSSION

Rainfall–discharge relation

The rainfall–discharge relation was determined using only measurements made in 2001 and 2002 for those

Published in 2007 by John Wiley & Sons, Ltd.

Table III. Summary of hydraulic functional conductivity calculations for subwatersheds burned by the 2000 Cerro Grande Fire

Watershed	2	3	4	9	11	13	14
Average ΔNBR of subwatershed	730	589	384	547	615	574	29
Number of random selected hillslope flow paths	13	14	20	10	9	18	44
Average area of all hillslope flow paths (30 m × 30 m pixels)	4·2	3·9	4·2	4·4	4·4	3·2	3·4
Average slope of all hillslope flow paths	0·40	0·51	0·51	0·56	0·49	0·33	0·14
Average length of all hillslope flow paths (m)	136	133	150	162	164	112	119
SD of length of all hillslope flow paths (m)	90	44	40	86	73	51	44
CV of length of all hillslope flow paths	0·66	0·33	0·27	0·53	0·45	0·46	0·37
Average sinuosity of all hillslope flow paths	1·03	1·02	1·05	1·04	1·03	1·04	1·05
Average ΔNBR for all hillslope flow paths	737	591	392	528	607	579	37
SD of ΔNBR for all hillslope flow paths	92	132	129	127	61	102	88
CV of ΔNBR for all hillslope flow paths	0·12	0·22	0·33	0·24	0·10	0·18	2·4
Average hydraulic functional connectivity Φ	6730	4650	2810	5790	5410	2410	91
SD of hydraulic functional connectivity Φ	8920	3300	1530	6210	3390	2490	233
CV of hydraulic functional connectivity Φ	1·33	0·71	0·54	1·07	0·63	1·03	2·6

ΔNBR: differenced normalized burn ratio; CV: coefficient of variation; SD: standard deviation.

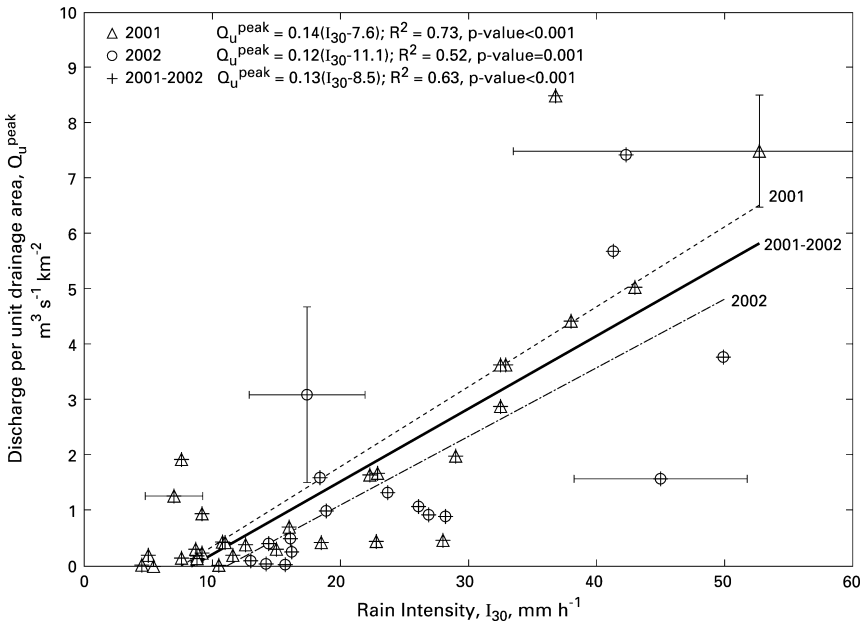

Figure 3. Rainfall–discharge relation for four subwatersheds in Rendija Canyon. The empirical regressions use only data collected in 2001, in 2002 and from subwatersheds 3, 9, 11, and 13 with approximately the same soil burn severity ΔNBR = 581 ± 5%. The uncertainty bars of I_{30} and Q^{peak} are indicated only for a few representative measurements. These bars represent plus/minus one standard deviation. For two measurements the uncertainty in discharge is smaller than the size of the symbol. The uncertainty for the remaining measurements is given in Table II. The dashed line represents the rainfall–runoff relation for 2001 and the dot–dashed line represents the relation for 2002. The solid line is the rainfall–runoff relation for the combined data set of 2001 and 2002

subwatersheds (3, 9, 11, and 13) with similar burn severity (ΔNBR = 581 ± 5%). Thus, the Q_u^{peak} only depended on I_{30}, not on ΔNBR (Figure 3). Discharges were not observed for some rainfall intensities. The rainfall–discharge relation was determined for 31 data pairs in 2001 and 17 data pairs in 2002. The linear relation between rainfall intensity I_{30} and Q_u^{peak} expressed in units of millimetres per hour can be written in the following convenient form:

$$Q_u^{peak} = b(I_{30} - I_{30}^{thres}) \quad I_{30} > I_{30}^{thres} \tag{12}$$

where $b = 0{\cdot}50$, $I_{30}^{thres} = 7{\cdot}6$ mm $h^{-1} = 7{\cdot}6$, $R^2 = 0{\cdot}73$, and $p < 0{\cdot}001$ for the 2001 data and $b = 0{\cdot}43$, $I_{30}^{thres} = 11{\cdot}1$ mm h^{-1}, $R^2 = 0{\cdot}52$, and $p = 0{\cdot}001$ for the 2002 data. The two values of I_{30}^{thres} (intercepts of the I_{30} axis) for Rendija Canyon (Figure 3) are within the range of estimates of I_{30}^{thres} values for individual subwatersheds (Table I); however, the two values are not significantly different based on the standard errors of the slope b and standard errors of the intercepts on the Q_u^{peak} axis (Figure 3). Therefore, the two data sets were combined together and the resulting linear regression gave $b = 0{\cdot}47$, $I_{30}^{thres} = 8{\cdot}5$ mm h^{-1}, $R^2 = 0{\cdot}63$, and $p < 0{\cdot}001$.

The rainfall threshold, I_{30}^{thres}, for this data set is similar to other reported thresholds. Reneau and Kuyumjian (2004) reported equivalent I_{30} values of 8·0 mm h^{-1} and 10·1 mm h^{-1} for 2001 and 2002 respectively for neighbouring Pueblo Canyon. Previous research (Doehring, 1968; Inbar *et al.*, 1998; Kunze and Stednick, 2006) measured rainfall-intensity thresholds that were 12·7 mm h^{-1}, 10 mm h^{-1}, 10 mm h^{-1} for watersheds (4–20 km^2) in

southern California, Israel, and northern Colorado respectively. Although the I_{30}^{thres} values reported in this paper for 2001 and 2002 are not statistically different as a result of the inherent rainfall and runoff variability, the higher value in 2002 may reflect the change in vegetation. Fire-adapted vegetation was observed to produce a new, rain-intercepting canopy by resprouts from roots and burned stumps within a few months (aspen, *Populus tremuloides*), within a year (locust, *Robinia neomexicana*, and oak, *Quercus gambelii*), or within 1–2 years from seed such as those of the Fendler buckbush (*Ceanothus fendleri*).

The runoff response after a fire is a transient process that changes in space and time and, therefore, is difficult to quantify with the certainty associated with uniform, steady-state flow. Several reasons contribute to this uncertainty of the rainfall–discharge relation (Equation (12) and Figure 3). The first, most obvious reason is the natural variability of the rainfall intensity, for which a few uncertainty intervals are indicated in Figure 3 and others are listed in Table II. A second reason is caused by having to use measurements with different time-scales. The measurements of Q_u^{peak} represent nearly instantaneous values, whereas I_{30} represents a time average over a 30 min interval. This longer interval of time may have shorter intervals with rainfall intensity greater than I_{30} embedded within it, which actually produces the measured Q_u^{peak}.

A third reason is that peak discharges produced by spatially variable rainfall falling on a subwatershed distant from the mouth of the subwatershed can be substantially attenuated by conveyance through the channel network. We observed two processes that can attenuate peak discharge: (1) spatial diffusion of the flood wave and (2) trapping of water in the bed as suspended sediment settles. These transmission losses have also been observed in neighbouring canyons (S. Reneau, personal communication, 2006). Measurements of the first process were made in 2000, and the peak discharges per unit channel width in the North and South Branches of Rendija Canyon (Figure 1) decreased from about 45 $m^3\ s^{-1}$ to about 20 $m^3\ s^{-1}$ over a distance of 2000 m during one flood. The second process was not measured directly, but was estimated using Darcy's law for subsurface flow in a porous medium (with typical thicknesses on the order of 0·5 m, widths of 10 m, slopes of 0·04, and permeabilities of 6×10^{-2} m s^{-1}). This estimate indicated at least a 10% decrease in Q_u^{peak} if Q_u^{peak} is less than 0·42 $m^3\ s^{-1}\ km^{-2}$, which was the case for 29% of the measurements (Table I) used to determine the rainfall–discharge relation.

A fourth reason is that the erosion and deposition of alluvial material at a discharge measurement site can induce large uncertainties in the cross-sectional area and, hence, in the peak discharge measurements. This was especially true in subwatershed 11, where the measurement location was at the mouth of the tributary close to the main channel. Large fluctuations in the level of the alluvial bed in this tributary depended on the level of water in the main channel. At times, flow in the main channel created backwater with a relatively flat water-surface slope connecting the tributary to the main channel and, thus, provided ideal conditions for deposition. At other times, when only subwatershed 11 received rainfall, the water-surface slope was steeper (B. Dunn, personal communication, 2001) and created sufficient shear stress to erode the alluvial bed.

Burn severity

The values of ΔNBR for 30 m pixels ranged from about −200 to +1000 within the entire Cerro Grande Fire perimeter. The distribution of ΔNBR values was bimodal, with one peak of about 100 and another peak between 300 and 600. This reflected the wide range of burn severities within the Cerro Grande Fire. In contrast,

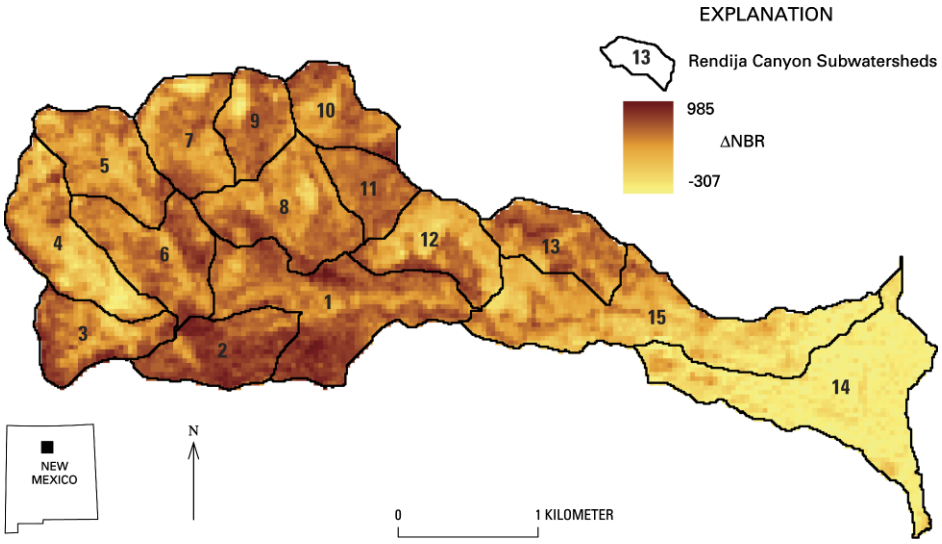

Figure 4. The spatial pattern of burn severity expressed as the change in the normalized burn ratio ΔNBR in subwatersheds of Upper Rendija Canyon (see Figure 1)

Rendija Canyon had a single peak in the distribution between 400 and 600, but the entire range extended from about −50 to 800 (Figure 4).

The ΔNBR values were correlated with burn severity indicators within the perimeter of the Cerro Grande Fire perimeter and within the subwatersheds in Rendija Canyon itself. The burn severity indicators were ground char ratings based on depth of ground char, amount and type of remaining litter, colour and texture of the mineral soil (Ryan and Noste, 1985), and stem char height. These were measured 1 year after the fire in June 2001 using 0·1 ha multiscale, modified-Whittaker vegetation plots (G. Chong, personal communication, 2004). The ΔNBR values ($n = 75$) at the centre point of the 20 m × 50 -m field plots and the burn severity indicators were positively correlated with coefficients of determination $R^2 = 0{\cdot}59$ and 0·60 for stem char height and depth of ground char respectively.

Runoff coefficient

Mean values of runoff coefficient and the hydraulic functional connectivity were computed for each subwatershed. The number of measurements in these means ranged from 6 to 13 (Table II), so that estimates of the variance of the means were also calculated. The variances were heteroscedastic; therefore, the weighted least-squares regression is the appropriate method to use (Draper and Smith, 1981; Helsel and Hirsch, 1992). This regression method uses both the mean and the variance (a measure of the reliability of the mean). The relation between C and Φ (Figure 5) using the weighted least-squares regression was

$$C = 4{\cdot}9 \times 10^{-5}\Phi + 0{\cdot}036 \qquad R^2 = 0{\cdot}87,\ p = 0{\cdot}002 \tag{13}$$

The sinuosities of the hillslope flow paths were not included in computing the hydraulic functional connectivity for Rendija Canyon. They were essentially unity (Table III) because the pixel scale approximating a flow path was much greater than the actual scale (1–2 m) of hillslope flow paths. Therefore, the sinuosity at this scale would have little effect. The sinuosity of the flow paths could be easily included if the resolution of the DEM were increased.

One possible problem with the hydraulic functional connectivity might be that some flow paths may cross outcrops of bedrock. For pixels with bedrock outcrops, the ΔNBR would be zero because there would be no change between reflectance measured before and after a fire. However, the average percentage of the drainage area covered by bedrock outcrops in the seven subwatersheds was 3·3% (Table I). Thus, bedrock outcrops in the study area do not have a significant effect on the hydraulic functional connectivity.

In addition to the linear relation between the means, there was a linear relation between the variances of C and Φ. The variability of the runoff coefficient $s(C)$ was related to the variability of the hydraulic functional connectivity $s(\Phi)$ by

$$s(C) = 4{\cdot}0 \times 10^{-5} s(\Phi) + 0{\cdot}074 \quad R^2 = 0{\cdot}76,\ p = 0{\cdot}01 \tag{14}$$

Thus, the hydraulic functional connectivity can predict both the mean runoff response and the variability of the runoff response from burned watersheds. For example, two storms may be 'identical' in terms of magnitude and have the same I_{30} (the storms would plot at the same location on the horizontal axis in Figure 5); however, the storms may have different spatial variability because of the spatial distribution of the rainfall intensities. Thus, different spatial distributions of rainfall intensity will affect a different combination of hillslope flow paths for the two 'identical' storms. These different combinations of flow paths can produce different runoff coefficients for what appears to be 'identical' storms when only magnitude is considered.

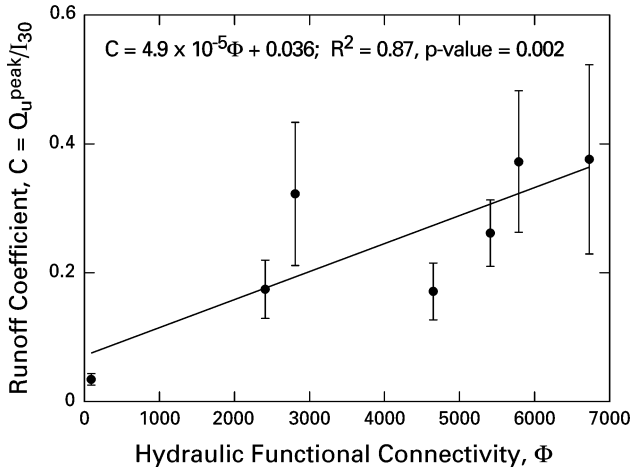

Figure 5. Relation between the runoff coefficient and the hydraulic functional connectivity. The vertical bars represent the standard error of the mean. The standard deviation of the burn severity and the hydraulic functional connectivity are given in Tables I and III

CONCLUSIONS

A linear rainfall–discharge relation was determined based on data from four small-scale (~0·28 km^2) subwatersheds in Rendija Canyon with nearly the same burn severity ΔNBR. The runoff was measured as the discharge per unit drainage area Q_u^{peak} and was found to be a linear function of the maximum 30 min rainfall intensity I_{30} with a rainfall-intensity threshold of 8·5 mm h^{-1}. Much of the uncertainty in this relation was created by the inherent natural variability in the rainfall intensities associated with summer convective rainfall. This unavoidable but large inherent uncertainty in the rainfall intensity at small scales is, in a sense, a hydrometeorological uncertainty principle that must be recognized in understanding the physical processes generating runoff in this type of rainfall regime. At larger scales, probably >100 km^2, runoff would be less variable as the variability of rainfall intensity would be averaged over a larger surface area.

Published in 2007 by John Wiley & Sons, Ltd.

DOI: 10.1002/hyp

The hydraulic functional connectivity is a burn severity variable that incorporates both the magnitude of the burn severity and the spatial sequence of the burn severity along hillslope flow paths. The results show that the mean runoff coefficient $C = Q_u^{peak}/I_{30}$ for seven subwatersheds was linearly related to the mean hydraulic functional connectivity Φ. Moreover, the variability of the runoff coefficient is related to the variability of the hydraulic functional connectivity and provides insight into why the runoff response from the same subwatershed can vary for two different storms with the same area-averaged rainfall intensity. These results provide verified relations based on quantitative field measurements for predicting peak discharges per unit drainage area from burned areas as a function of burn severity.

ACKNOWLEDGMENTS

Measuring rainfall and stream discharge in rugged mountainous terrain is not a four-person effort. We are deeply appreciative for the help and muscles of Erica Bigio, Brian Ragan, Joe Gartner, and John Gartner in deploying, maintaining, downloading, and recovering data from the rain-gauges and stream gauges in Rendija Canyon. John Hogan organized a special group of volunteers (Elizabeth Bennett, Sarah Buehrer, Kevin Buckley, Helen Dahlby, Patricia Danforth, Richard Danforth, Bill Dunn, Ian Dunn, Janet Gerwin, Robert Greene, Eric Henderson, Gloria Lopez, Laura McClellan, David Modl, Markus Mueller, and Jennifer Rezmer) from Los Alamos, New Mexico, to maintain a network of visual rain-gauges and crest-stage gauges, which they read each day. This provided us with verification of our measurements and an invaluable alert system that told us when these elusive floods had happened and when we needed to make crucial field measurements. Discussions with Greg Kuyumjian were definitely educational and expanded our thinking. Greg, Steve Reneau and many other anonymous reviewers also provided many thought-provoking comments on early versions of the paper. Any use of trade, product, or firm names in this paper is for descriptive purposes only and does not constitute endorsement by the US Government.

REFERENCES

Abrahams AD, Parsons AJ, Luk SH. 1986. Resistance to overland flow on desert hillslopes. *Journal of Hydrology* **88**: 343–363.

BAER. 2000. *Cerro Grand Fire, Burned Area Emergency Rehabilitation (BAER) plan*. Interagency BAER Team: Los Alamos, NM.

BAER. 2002. *Coal seam fire, burned area emergency stabilization and rehabilitation plan*. US Forest Service, White River National Forest, Glenwood Springs, CO.

Barfield BJ, Warner RC. 1985. *Applied Hydrology and Sedimentology for Disturbed Areas.* Oklahoma Technical Press: Stillwater, OK; 57–69.

Bathurst JC. 1985. Flow resistance estimation in mountain rivers. *Journal of Hydraulic Engineering* **111**: 625–643.

Benavides-Solorio JD, MacDonald LH. 2005. Measurement and prediction of post-fire erosion at the hillslope scale, Colorado Front Range. *International Journal of Wildland Fire* **14**: 1–18.

Bonnin GM, Todd D, Lin B, Parzybok T, Yerta M, Riley D. 2004. *Precipitation–Frequency Atlas of the United States, NOAA Atlas 14, Volume 1, Semiarid Southwest (Arizona, Southeast California, Nevada, New Mexico, Utah)*. National Weather Service: Silver Spring, MD.

Bowen BM. 1990. *Los Alamos climatology*. Los Alamos National Laboratory Report LA-11735-MS.

Chow VT. 1964. *Handbook of Applied Hydrology*. McGraw-Hill: New York, NY.

Cocke AE, Fulé PZ, Crouse JE. 2005. Comparison of burn severity assessments using differenced normalized burn ratio and ground data. *International Journal of Wildland Fire* **14**: 189–198.

Darboux F, Davy P, Gascuel-Odoux C, Huang C. 2001. Evolution of soil surface roughness and flowpath connectivity in overland flow experiments. *Catena* **46**: 125–139.

Davenport DW, Breshears DD, Wilcox BP, Allen CD. 1998. *Journal of Range Management* **51**: 231–240.

DeBano LF. 2000. The role of fire and soil heating on water repellency in wildland environments: a review. *Journal of Hydrology* **231–232**: 194–206.

Doehring DO. 1968. The effect of fire on geomorphic processes in the San Gabriel Mountains, California. *Contributions to Geology* **7**: 43–65.

Doerr SH, Shakesby RA, Blake WH, Chafer CJ, Humphreys GS, Wallbrink PJ. 2006. Effects of differing wildfire severities on soil wettability and implications for hydrological response. *Journal of Hydrology* **319**: 295–311.

Draper NR, Smith H. 1981. *Applied Regression Analysis*. Wiley: New York, NY; 108–109.

Feldman AD. 2000. HEC-1 Flood Hydrograph Package. In *Computer Models of Watershed Hydrology*, Singh VP (ed.). Water Resources Publications: Highlands Ranch, CO; 119–150.

Gilley JE, Flanagan DC, Kottwitz ER, Weltz MA. 1992. Darcy–Weisbach roughness coefficients for overland flow. In *Overland Flow: Hydraulic and Erosion Mechanics*, Parsons AJ Abrahams AD (eds). Chapman & Hall: New York, NY; 25–52.

Goodrich DC, Faurès JM, Woolhiser DA, Land LJ, Sorooshian S. 1995. Measurement and analysis of small-scale convective storm rainfall variability. *Journal of Hydrology* **173**: 283–308.

Grant GE. 1997. Critical flow constrains flow hydraulics in mobile-bed stream: a new hypothesis. *Water Resources Research* **33**: 349–358.

Hawkins RH. 1973. Improved prediction of storm runoff in mountain watersheds. *Journal of the Irrigation and Drainage Division, Proceedings of the American Society of Civil Engineers* **99**: 519–523.

Hawkins RH, Cundy TW. 1987. Steady-state analysis of infiltration and overland flow for spatially-varied hillslopes. *Water Resources Bulletin* **23**: 251–256.

Helsel DR, Hirsch RM. 1992. *Statistical Methods in Water Resources*. Elsevier: Amsterdam; 280–283.

Hershfield DM. 1961. *Rainfall Frequency Atlas of the United States for Duration from 30 Minutes to 24 Hours and Return Periods from 1 to 100 Years.* US Department of Commerce.

Huff FA. 1979. *Spatial and temporal correlation of precipitation in Illinois*. Illinois State Water Survey, Illinois Institute of Natural Resources Circular 141.

Inbar M, Tamir M, Wittenberg L. 1998. Runoff and erosion processes after a forest fire in Mount Carmel, a Mediterranean area. *Geomorphology* **24**: 17–33.

Interagency Advisory Committee on Water Data. 1981. *Guideline for determining flood flow frequency*. US Geological Survey Bulletin 17B.

Jarrett RD. 1987. Errors in slope–area computations of peak discharges in mountain streams. *Journal of Hydrology* **96**: 53–67.

Key CH, Benson NC. 2005. Landscape assessment: ground measure of severity, the Composite Burn Index; and Remote sensing of severity, the Normalized Burn Ratio. In *FIREMON: Fire Effects Monitoring and Inventory System*, Lutes DC, Keane RE, Caratti JF, Key CH, Benson NC, Sutherland S, Gangi LJ (eds). Rocky Mountain Research Station General Technical Report RMRS-GTR-164-CD. US Department of Agriculture, Forest Service: Ogden, UT; LA1–51.

Kunze MD, Stednick JD. 2006. Streamflow and suspended sediment yield following the 2000 Bobcat Fire, Colorado. *Hydrological Processes* **20**: 1661–1681.

Kutiel P, Lavee H, Segev M, Benyamini Y. 1995. The effect of fire-induced surface heterogeneity on rainfall–runoff–erosion relationships in an eastern Mediterranean ecosystem, Israel. *Catena* **25**: 77–87.

Martin DA, Moody JA. 2001. Comparison of soil infiltration rates in burned and unburned mountainous watersheds. *Hydrological Processes* **15**: 2893–2903.

May DR, Julien PY. 1998. Eulerian and Lagrangian correlation structures of convective rainstorms. *Water Resources Research* **34**: 2671–2683.

McGarigal K, Cushman SA, Neel MC, Ene E. 2002. *FRAGSTATS: Spatial Pattern Analysis Program for Categorical Maps*. Computer software program produced by the authors at the University of Massachusetts, Amherst. www.umass.edu/landeco/research/fragstats/fragstats.html [March 2007].

Miller JD, Nyhan JW, Yool SR. 2003. Modeling potential erosion due to the Cerro Grande Fire with a GIS-based implementation of the revised universal soil loss equation. *International Journal of Wildland Fire* **12**: 85–100.

Miller JF, Frederick RH, Tracey RJ. 1973. *Precipitation–Frequency Atlas of the Western United States, Volume III–Colorado*. National Oceanic and Atmospheric Administration, National Weather Service.

Moody JA, Martin DA. 2001a. *Hydrologic and sedimentologic response of two burned watersheds in Colorado*. US Geological Survey Water-Resources Investigations Report 01–4122.

Moody JA, Martin DA. 2001b. Post-fire, rainfall intensity-peak discharge relation for three mountainous watersheds in the western USA. *Hydrological Processes* **15**: 2981–2993.

Moody JA, Smith DJ, Ragan BW. 2005. Critical shear stress for erosion of cohesive soils subjected to temperature typical of wildfires. *Journal of Geophysical Research* **110**: 1–13.

Moore ID, Foster GR. 1990. Hydraulics and overland flow. In *Process Studies in Hillslope Hydrology*, Anderson MG, Burt TP (eds). Wiley: New York, NY; 215–254.

Morin J, Kosovsky A. 1993. Infiltration of natural rain. In *Evaluating and predicting the spatial and temporal variability of storm runoff generation in watersheds of arid and semi-arid regions*, Morin J (ed.). Final report of BARD Research Project 1, 1486–88; 85–108.

Nachabe MH, Illangasekare TH, Morel-Seytour HJ, Ahuja LR, Ruan H. 1997. Infiltration over heterogeneous watersheds: influence of rain excess. *Journal of Hydrologic Engineering* **2**: 140–143.

National Wildfire Coordinating Group. 1994. *Glossary of wildland fire terms*. Publication PMS 205/NFES 1832. National Interagency Fire Center: Boise, ID.

NRCS. 1986. *Urban hydrology for small watersheds*. US Department of Agriculture, Natural Resources Conservation Services, Technical Release 55.

Peterson GD. 2002. Contagious disturbance, ecological memory, and the emergence of landscape pattern. *Ecosystems* **5**: 329–338.

Reneau SL, Kuyumjian GA. 2004. *Rainfall–runoff relations in Pueblo Canyon, New Mexico, after the Cerro Grande Fire*. Los Alamos National Laboratory Report LA-UR-04-8810.

Reneau SL, Kuyumjian GA, Malmon DV, Tardiff MF. 2003. *Precipitation–frequency relations on the Pajarito Plateau and in the eastern Jemez Mountain, New Mexico, and examples of extreme or flood-producing storms*. Los Alamos National Laboratory Report LA-UR-03-6484.

Ries III KG, Crouse MY. 2002. *The national flood frequency program, version 3: a computer program for estimating magnitude and frequency of floods for ungaged sites*. US Geological Survey Water-Resources Investigations Report 02-4168.

Robichaud PR, Waldrop TA. 1994. A comparison of surface runoff and sediment yields from low- and high-severity site preparation burns. *Water Resources Bulletin* **30**: 27–34.

Rowe PB, Countryman CM, Storey HC. 1954. *Hydrologic analysis used to determine effects of fire on peak discharge and erosion rates in Southern California watersheds*. US Department of Agriculture, Forest Service, California Forest and Range Experiment Station.

Ryan KC, Noste N. 1985. Evaluating prescribed fires. In *Symposium and Workshop on Wilderness Fire*, Lotan JE, Kilgore BM, Fischer WC, Mutch RW (technical coordinators): Missoula, MT.

Smith RE, Smettem KRJ, Broadbridge P, Woolhiser DA. 2002. *Infiltration Theory for Hydrologic Applications*. *Water Resources Monograph* 15. American Geophysical Union; Washington, DC.

Sorbel B, Allen J. 2005. Space-based burn severity mapping in Alaska's National Parks. In *Connections to Natural and Cultural Resource Studies in Alaska's National Park*, Shah M (ed.). Alaska Park Science **4**: 5–11.

Zinke PJ. 1967. Forest interception studies in the United States. In *Forest Hydrology*, Sopper WE Lull HW (eds). Pergamon Press: New York, NY; 137–161.